

The Star Formation History in a Hierarchical Universe

Rachel S. Somerville ¹, Joel R. Primack ²

¹ *Racah Institute of Physics, The Hebrew University, Jerusalem 91904, Israel*

² *Physics Department, University of California, Santa Cruz, CA 95060 USA*

Abstract

Observations now probe the star formation history of the Universe back to a redshift of $z \sim 5$. We investigate whether the predictions of semi-analytic models of galaxy formation based on hierarchical Cold Dark Matter (CDM) type models are in agreement with these direct observations and also with the “fossil” evidence contained in constraints on the ages of present day early-type galaxies. Previous models [1] predicted that the star formation rate density falls off rather steeply at $z \gtrsim 2$, and correspondingly that the majority of the stars in the Universe formed at relatively low redshift. We investigate the effect of including a bursting mode of star formation, assuming that galaxy-galaxy mergers trigger starbursts and using the merger rate that arises naturally in the CDM merging hierarchy. The resulting starbursts substantially increase the global star formation rate at high redshift, leading to predictions that are in good agreement with the star formation rate density at $z \sim 3$ obtained from sub-millimeter observations (SCUBA) and optical/UV estimates after correction for dust extinction. The mass of stars formed at $z \geq 3$ is correspondingly in better agreement with the fossil evidence. We also investigate complementary global quantities such as the mass of cold gas and the average metallicity of cold gas as a function of redshift, and the integrated extra-galactic background light. We argue that these observations, taken together, provide strong constraints on the star formation history of the Universe, and that hierarchical models of the CDM type are in reasonable agreement with these observations when starbursts are included.

1 Introduction

The star formation history of the Universe has been observationally probed using many approaches, both direct and indirect. The star formation rate density has been derived from direct observations using a variety of tracers such as $H\alpha$ [2, 3, 4], [OII] [5], or UV emission [6, 7, 8]. Recently, sub-mm observations obtained with the SCUBA instrument were used to estimate the star formation rate at $z \sim 3$ [9]. The compilation of these observations, which extend from $z = 0$ to $z \sim 5.5$, sketches out an enticing picture of the history of star formation and have come to be referred to generically as “the Madau diagram” [7]. However, the interpretation of the Madau diagram is not necessarily straightforward. Because of dust extinction, the optical and UV tracers certainly underestimate the true star formation rate, but by an uncertain factor. The sub-mm flux observed by SCUBA is due to the re-radiation of light that was absorbed by dust at shorter wavelengths, and so provides a useful complement to the optical and UV observations. However, the low resolution of the SCUBA instrument makes it difficult to find

unique optical counterparts and measure redshifts to the sources. The measurement of the mass density in the form of cold gas as a function of redshift, derived from observations of damped Lyman- α systems [10, 11], provides an indirect and complementary indicator of the star formation history [12], as does the measurement of the average metal content of these systems at various redshifts [13]. The extragalactic background light (EBL), which has been measured from the UV to the sub-mm (reviewed by [14]), is another indirect constraint which may prove to be quite powerful, because it effectively measures the bolometric luminosity density. An alternative method of determining the star formation history of the Universe, discussed by A. Renzini at this meeting and elsewhere [15], is to use “fossil evidence” such as the age constraints derived from the small scatter in the observed color-magnitude and fundamental plane relations for early type galaxies and galactic bulges out to $z \simeq 0.5$ (extensive references are given in [15]).

A recurring theme of this meeting, and indeed an important question in the study of galaxy formation today, is whether any existing theoretical framework can fit these observations into a self-consistent picture. This is a difficult question, as in order to model these quantities one is forced to consider messy astrophysical processes such as gas dynamics, star formation, supernovae feedback, and absorption and re-radiation by dust. Currently, the only efficient way to do this is using semi-analytic models such as those developed in e.g. [16], [17], and [18]. Previous work (e.g., [17, 1]) has left the impression that a “late epoch of star formation” (i.e., the peak in the global star formation history at $z \sim 1.5 - 2$ and a steep decline at higher redshifts) is a generic feature of CDM-type models. This behaviour is similar to the star formation history sketched out in the original Madau diagram [7], and has been claimed as a success of these models.

However, there is mounting evidence that the true star formation rate history at $z \gtrsim 3$ may be considerably different from the original estimates. This could be due to a number of effects, including dust extinction, a steeper slope on the faint end of the luminosity function (suggested by the results of [19] based on photometric redshifts in the HDF), or unknown selection effects intrinsic to the Lyman-break selection technique. The revised star formation rate density may well be consistent with the SCUBA lower limit at $z = 3$. Moreover, as pointed out by Renzini, the integration of the original Madau diagram, like the models of Ref. [1] which have a similar star formation history, would predict that only about 5 percent of the stars in galaxies today formed before a redshift of three, in fairly serious disagreement with the fossil evidence (Renzini has argued that ~ 30 percent of the stars in galaxies today formed before $z = 3$, if cluster galaxies are typical). This might seem to indicate a serious problem with the entire hierarchical, CDM-based picture of structure formation.

However, it turns out that a natural feature of the CDM merging hierarchy, neglected in previous work, can change the situation significantly. This feature is the star formation occurring in starbursts triggered by galaxy-galaxy mergers. We first became interested in this idea as a way to explain the very large luminosities and high star formation rates of the physically small Lyman-break galaxies [20], which it seems to do very successfully. In the remainder of this paper, we will summarize the implications of the starburst model for the properties of Lyman-break galaxies (LBGs), as well as for the global star formation rate density, cold gas density, and metal content of the Universe as a function of redshift. We will conclude that in fact the classic CDM picture is in good agreement with all these observations within the present uncertainties.

2 Semi-analytic models of galaxy formation

Semi-analytic techniques allow one to model the formation and evolution of galaxies in a hierarchical framework, including the effects of gas cooling, star formation, supernova feedback, chemical evolution, galaxy-galaxy merging, and the evolution of stellar populations. The semi-analytic models used here are described in detail in [21], [18], and [20]. These models are in reasonably good agreement with a broad range of local galaxy observations, including the Tully-Fisher relation, the B-band luminosity function, cold gas contents, metallicities, and colors [18]. Our basic approach is similar in spirit to the models originally developed by the Munich [16] and Durham [17] groups, and subsequently elaborated by these groups in numerous other papers (reviewed in [21] and [18]). Significant improvements included in [18] are that we assumed a lower stellar mass-to-light ratio (in better agreement with observed values), included the effects of dust extinction (which are significant in the B-band), and developed an improved “disk-halo” model for supernovae feedback. With these new ingredients, we simultaneously produce a Tully-Fisher relation with the correct zero-point and slope, and a B-band luminosity function with approximately the right normalization and shape on the bright and faint ends.

The framework of the semi-analytic approach is the “merging history” of a dark matter halo of a given mass, identified at $z = 0$ or any other redshift of interest. We construct Monte-Carlo realizations of halo “merger trees” using the method described in [22]. Each branch in the tree represents a halo merging event. When a halo collapses or merges with a larger halo, we assume that the associated gas is shock-heated to the virial temperature of the new halo. This gas then radiates energy and cools. The cooling rate depends on the density, metallicity, and temperature of the gas. Cold gas is turned into stars using a simple recipe, and supernova energy reheats the cold gas according to another recipe. Chemical evolution is traced assuming a constant yield of metals per unit mass of new stars formed. The spectral energy distribution (SED) of each galaxy can then be obtained by assuming an IMF and using stellar population models (e.g. [23]; here we use the GISSEL98 models with solar metallicity). It is then straightforward to obtain magnitudes and colours in any desired filter band. Our recipes for star formation, feedback, and chemical evolution contain free parameters, which are set by requiring an average fiducial “reference galaxy” (the central galaxy in a halo with a circular velocity of 220 km s^{-1}) to have an I-band magnitude $M_I - 5 \log h = -21.7$ (this requirement fixes the zero-point of the I-band Tully-Fisher relation to agree with observations), a cold gas mass $m_{\text{cold}} = 10^{10} h^{-2} M_{\odot}$, and a stellar metallicity of about solar. The star formation and feedback processes are some of the most uncertain elements of these models, and indeed of any attempt to model galaxy formation. We have investigated several different combinations of recipes for star formation and supernova feedback (sf/fb) and also several cosmologies, discussed in detail in [18] and [20], but here we will discuss results for a single choice of sf/fb recipe (constant efficiency quiescent star formation and the “disk-halo” feedback model) and cosmology ($\sigma_8 = 0.67$ SCDM), and a standard Salpeter IMF.

2.1 Modeling starbursts

We start with the ansatz that galaxy-galaxy mergers trigger starbursts. This premise has considerable observational support and is also supported by N-body simulations with gas dynamics and star formation [24]. In our models, galaxies that are within the same large halo may merge according to two different processes. Satellite galaxies lose energy and spiral in to the center of the halo on a *dynamical friction* time-scale. In addition, satellite galaxies orbiting within the same halo may merge with one another according to a modified *mean free path* time-scale. Our modeling of the latter process is based on the scaling formula derived in [25] to describe the

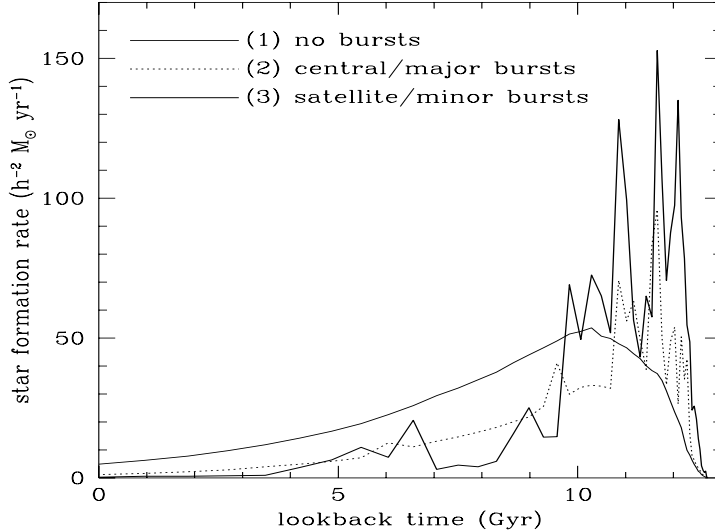


Figure 1: The total star formation rate for all galaxies that end up within a typical halo with $V_c = 500 \text{ km s}^{-1}$ at $z = 0$. The solid line shows a model (1) with no starbursts, the dotted line shows a model (2) with mergers only between satellite and central galaxies and bursts only in major mergers, and the dashed line shows a model (3) with satellite-satellite and satellite-central mergers and bursts in major and minor mergers. The lookback time is computed for $\Omega = 1$ and $H_0 = 50 \text{ km s}^{-1} \text{ Mpc}^{-1}$. Note that the peaks, representing starbursts, occur primarily at lookback times of 8 to 12 Gyr (redshifts $z \sim 1 - 5$).

results of dissipationless N-body simulations in which galaxy-galaxy encounters and mergers were simulated, covering a large region of parameter space.

When any two galaxies merge, the “burst” mode of star formation is turned on, with the star formation rate during the burst modeled as a Gaussian function of time. The burst model has two adjustable parameters, the time-scale of the burst and the efficiency of the burst (the fraction of the combined cold gas reservoir of both galaxies that is turned into stars over the duration of the burst). The timescale and efficiency parameters that we use are based on the simulations [24] mentioned above, treating major ($m_{\text{smaller}}/m_{\text{larger}} > f_{\text{bulge}} \sim 0.3$) and minor mergers separately. Details are given in [20]. The results of including bursts in a single halo with $V_c = 500 \text{ km s}^{-1}$ at $z = 0$ are shown in Fig. 1.

2.2 Comoving number density

Fig. 2 shows the comoving number density of galaxies brighter than a fixed magnitude limit (at rest $\sim 1500 \text{ \AA}$) as a function of redshift. Fig. 2 shows that models without bursts underpredict the number density of bright galaxies, while the burst models reproduce or exceed the observed number densities. Although tuning the free parameter that governs the efficiency of quiescent star formation can shift these curves up or down, the steep dependence on redshift is a generic feature of the quiescent models. Similarly, the flatter dependence arising in the burst models is due to several physical effects and is not sensitive to the values of the free parameters. The galaxy-galaxy merger rate is higher at higher redshift, and galaxies are more gas-rich and produce brighter starbursts. In addition, following [24], we suppress the starburst mode in bulge-dominated systems, which become more common at lower redshift.

Internal extinction due to dust is likely to be important, but the amount of dust and the resulting extinction are quite uncertain. The mean correction factors at rest 1500 \AA estimated

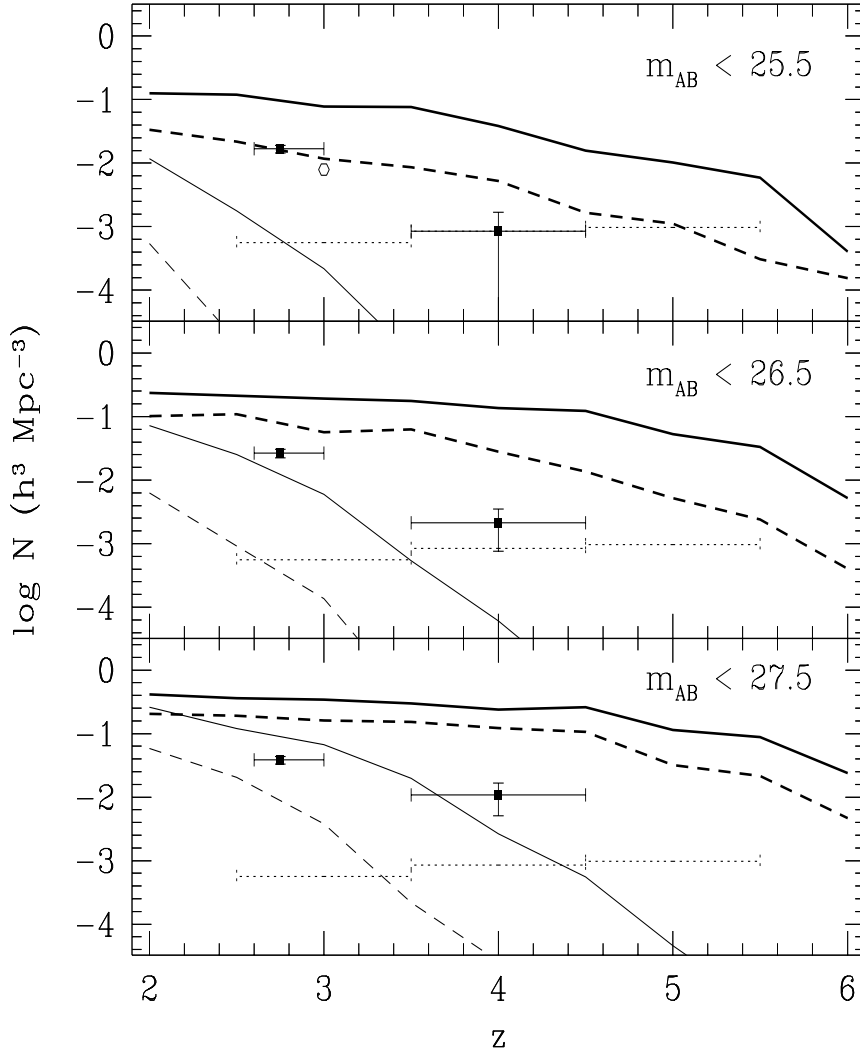


Figure 2: The comoving number density of galaxies brighter than $m_{AB} = 25.5$ (top panel), 26.5 (middle panel), and 27.5 (bottom panel), where $m_{AB} = (V_{606} + I_{814})/2$. The open hexagon indicates the comoving number density of LBGs from the ground-based sample of Steidel et al. [29]. The filled squares at $z = 2.75$ and $z = 4$ indicate the number density of U and B drop-outs (respectively) in the HDF [30]. The dashed horizontal lines correspond to one galaxy in the HDF volume for the indicated redshift intervals. Bold solid lines show the comoving number density of galaxies in the SCDM models with starbursts; light solid lines show the results of the no-burst models. Dashed lines show the result of reducing the flux of each galaxy by a factor of three to estimate the effects of dust extinction. In the no-burst models, the comoving number density of bright LBGs decreases rapidly with increasing redshift. The burst models predict that the comoving number density at $z = 4$ is nearly as high as at $z = 3$.

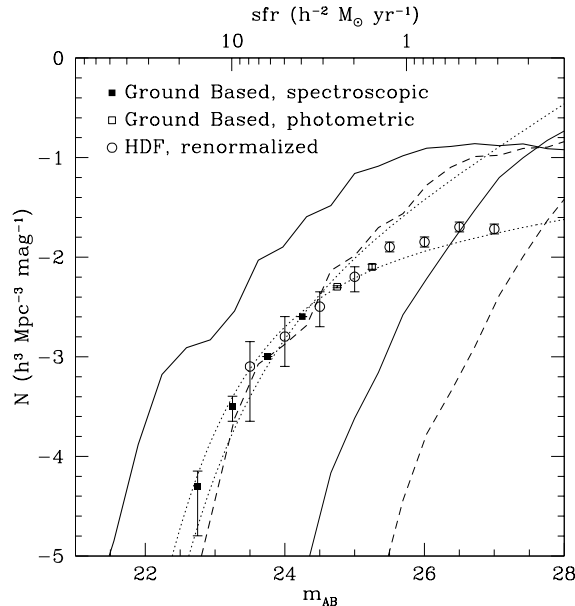


Figure 3: The luminosity function at $z = 3$ in the SCDM cosmology. Symbols show the composite luminosity function derived by [27] from the combined ground-based and HDF samples, and the dotted line shows the Schechter fit to these results ($\alpha = -1.3$). A Schechter function with a steeper slope, as found by [19], is also shown. Bold lines indicate the results of the models with starbursts, and light lines indicate the results of the no-burst models. The dashed lines show the results of a factor of three correction for dust extinction.

by Refs. [26, 27, 28] range from ~ 2 to ~ 7 . More dramatic corrections, as large as a factor of ~ 20 , have been suggested [31, 32]. At this meeting, C. Steidel reported that the net correction currently favored by his group is a factor of ~ 7 for the $\mathcal{R} < 25.5$ LBGs, but that the extinction is strongly differential, i.e. intrinsically brighter galaxies suffer larger extinctions. Here we have shown a conservative estimate of the effects of dust, by simply decreasing the luminosity of each galaxy by a factor of three. After this correction, the no-burst models fail quite dramatically, while the burst models still appear to be doing rather well.

Fig. 3 shows the rest 1500 \AA luminosity function (equivalently, the star formation rate distribution) at $z = 3$. The luminosity function in the no-burst models is a steep power-law. Increasing the efficiency of quiescent star formation would move the curve to the left, but the function is the wrong shape. More realistic, differential dust extinction would only exacerbate this problem. In the burst models, the shape of the uncorrected luminosity function is very similar to the one obtained by [27] from a combination of ground based and HDF data. With a factor of three correction for dust extinction, the burst models are consistent with the steeper luminosity function ($\alpha = -2.1$) obtained by [19] from the HDF.

Although the burst models are consistent with the observations when we include the conservative factor of three correction for dust extinction, the larger corrections and strong differential extinction now favored by the observers would destroy this good agreement. However, the remaining uncertainties are large enough that we should not be too concerned about this. If the basic starburst scenario is correct, the UV light that allows us to identify the LBGs is produced by young, high mass, and probably low metallicity stars. There are large uncertainties in the stellar population models in this regime, and the results are also highly sensitive to the IMF. In addition, although we have used the best information available to calibrate our treatment of galaxy-galaxy mergers and starbursts, the modelling should be improved. We [33] are currently investigating the frequency and spatial distribution of halo collisions in very high resolution

N-body simulations (based on the method of [34]). We are also extending the studies of gas dynamics and star formation in interacting galaxies using the same approach as [24]. We will cover a larger region of parameter space, and use galaxy properties more appropriate to the high redshift systems we are interested in [35].

2.3 Line-widths, ages, and stellar masses

The velocity dispersions of observed LBGs can be estimated based on the widths of nebular emission lines such as $H\beta$. Emission lines have been detected for a few of the brightest LBGs from the ground-based sample. The velocity dispersions σ derived from the observed linewidths are $\sigma = 60 - 80 \text{ km s}^{-1}$ for four objects, and $\sim 190 \text{ km s}^{-1}$ for one object [36]. These values agree well with the burst models, but are in strong disagreement with the no-burst models, which peak at $\sigma \sim 180 \text{ km s}^{-1}$ [20]. These measurements may be affected by several biases, which remain to be unravelled. Linewidths have been obtained only for the brightest LBGs, which may have systematically higher internal velocities. This would increase the discrepancy with no-burst models. The modelling of the velocity dispersion at the small radii probed by the observations (approximately the half-light radius) is also uncertain.

The ages and stellar masses of the burst models [20] also agree well with estimates based on multicolor photometry. LBG colors are well fit by young ($< 0.1 \text{ Gyr}$) stellar populations with moderate amounts of dust [32]. These young ages imply that stellar masses are also low ($\sim 10^9 M_\odot$). The LBGs in our no-burst models (and Ref. [1]) are systematically older and more massive than the data indicate. More photometry and spectra of LBGs will help to clarify whether models including starbursts adequately describe the properties of the LBGs.

2.4 Clustering

The large ground-based sample of LBGs, with many hundreds of spectroscopic redshifts, has made it possible to study the clustering of these objects. This data has provided several indications that the LBGs at $z \sim 3$ are strongly clustered: there are large “spikes” in redshift space [37], and the comoving correlation length (r_0) obtained from counts in cells is comparable to that of present day bright galaxies [38, 29]. Using dissipationless N-body simulations, and assuming that one LBG is associated with every halo above a mass threshold chosen in order to obtain the observed number density of LBGs, the probability of finding a spike as large as the one reported by [37] is then fairly large for several CDM cosmologies, including both $\Omega = 1$ and low- Ω variants [39]. The auto-correlation function for these halos also has a slope (γ) and correlation length (r_0) similar to the observations [29, 38]. Similar results have been obtained by several other groups (e.g. [40], [29]). It is clear from this work that if the LBGs are associated with fairly massive halos ($10^{11} - 10^{12} h^{-1} M_\odot$, depending on the cosmology and power spectrum) they will exhibit the observed strong clustering. The general population of halos with much smaller masses is much less strongly clustered. The burst models predict that LBGs may be found in halos with masses as small as $\sim 10^{11} M_\odot$, and based on the results of the studies mentioned above, this might appear to be in conflict with the observations. However, because the starbursts “turn on” for a relatively short period of time ($\sim 50 \text{ Myr}$), in our picture most of the LBGs are associated with halos that are merging or have experienced a very recent merger. When we identify halo collisions in very high resolution N-body simulations, we find that most collisions with enough baryons to produce a bright starburst involve relatively small mass halos located in dense regions [33]. Not surprisingly then, we find that merging or recently-merged halos are more strongly clustered than the overall population.

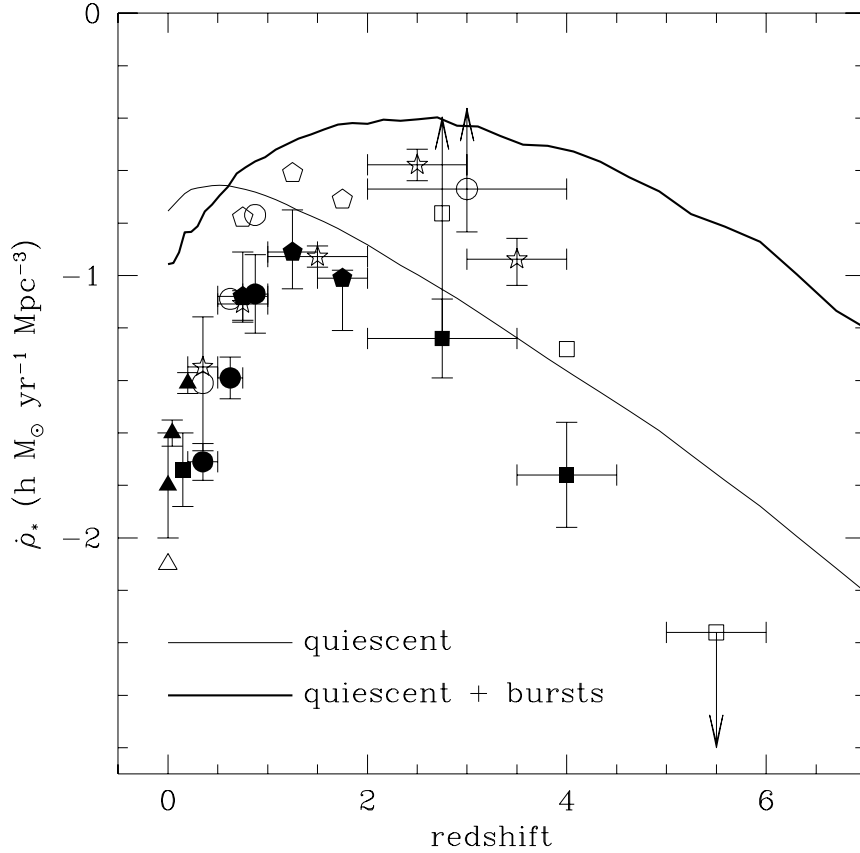


Figure 4: The star formation rate density as a function of redshift. The filled triangle at $z = 0$ is from H α observations of local galaxies [2], with the conversion from H α flux to star formation rate from Ref. [41]. The open triangle shows the star formation rate from the same observations, with the conversion factor originally used in Ref. [2]. The filled triangle at $z \sim 0.04$ is from new H α observations by the KISS survey [4], and the filled triangle at $z \sim 0.2$ is from H α observations of galaxies from the CFRS [3]. The filled square at $z \sim 0.15$ is from 2000 \AA fluxes from the UV survey of [8]. Filled circles are determined from the 2800 \AA fluxes of CFRS galaxies [6], and filled hexagons from the 2800 \AA flux of galaxies in the HDF using photometric redshifts [42]. The star symbols are from HDF photometric redshifts derived by Ref. [19]. Filled squares at $z = 2.75$ and $z = 4$ are from the ~ 1500 \AA fluxes of U- and B-dropouts in the HDF [7]. The open symbols show a correction for dust extinction of a factor of two for 2800 \AA flux and three for 1500 \AA flux, as suggested by [26]. The tip of the vertical arrow at $z \sim 3$ shows a correction of a factor of seven, which may be indicated by recent observational studies of dust extinction in LBGs (C. Steidel, this meeting). The large open circle at $z = 3$ shows the lower limit from the SCUBA observations of the HDF region [9] (assuming that these sources are stellar rather than AGN). Note that the discrepancy between the predictions and the data at low redshifts ($z \lesssim 1$) is partly alleviated when the models are corrected downward by about a factor of 2, to correct for the overprediction of the number density of $M \lesssim 0.1 M_*$ halos in the Press-Schechter approximation [43, 44]. This correction will also bring the predicted cold gas mass at $z \lesssim 1$ into better agreement with the observations (Fig. 6).

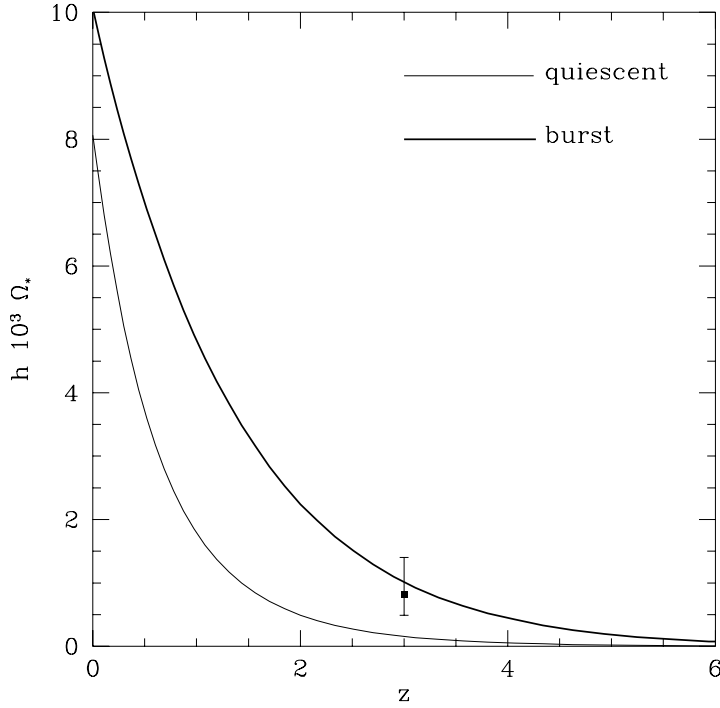


Figure 5: The stellar density (in units of the present critical density) as a function of redshift, in the quiescent (light line) and quiescent + burst (bold line) models. The data point shows the approximate stellar density at $z = 3$ obtained from “fossil evidence” (e.g. [15]).

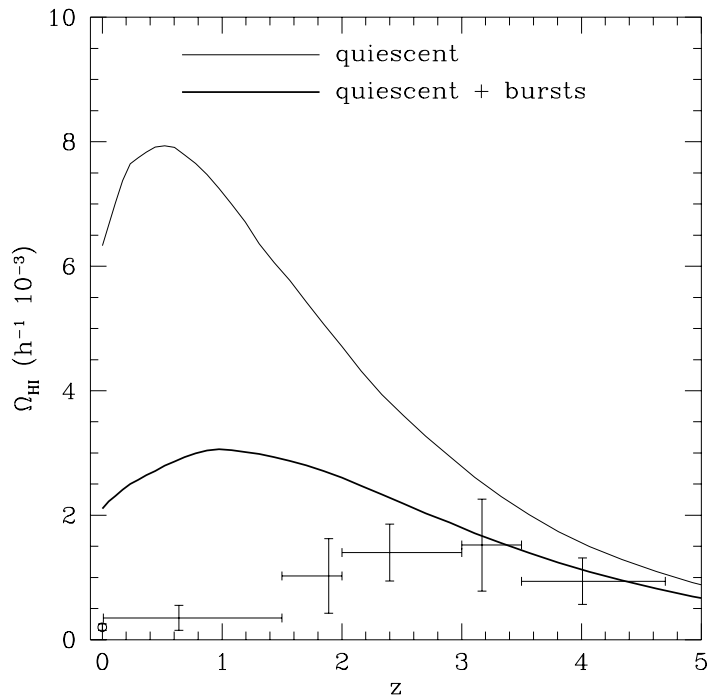


Figure 6: The evolution of the mass density of cold gas as a function of redshift. Data points show the density in the form of H_I estimated from observations of DLAS [11]. The data point at $z = 0$ is from local H_I observations [45]. Bold solid lines correspond to models including bursts, and light lines show the quiescent models.

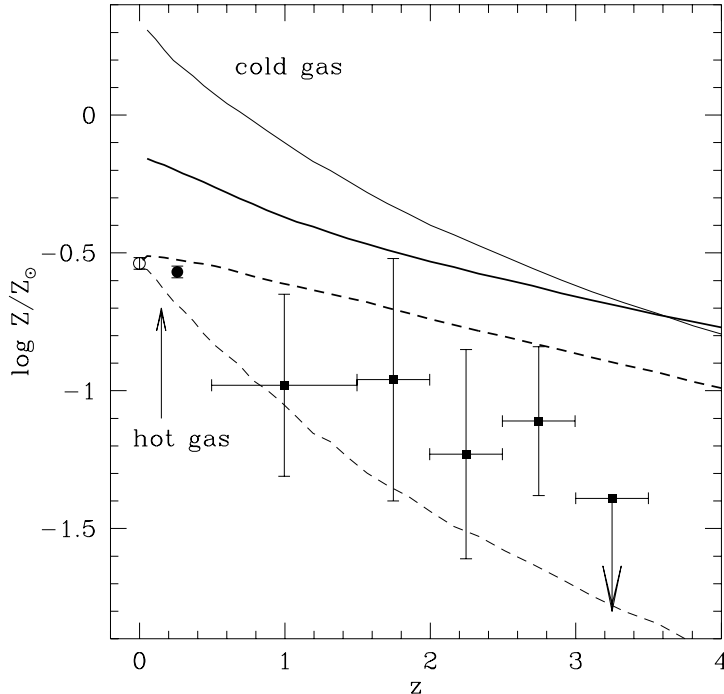


Figure 7: Metal content of the Universe. The square symbols are from the measurements of Zn abundance in DLAS ($[Zn/H_{\text{DLAS}}]$) from [13]. Circular symbols show the metallicity of hot gas from X-ray observations [46]. Light lines show the no-burst models and bold lines show the models including starbursts. Solid lines show the metallicity of cold gas in the models, and dashed lines show the metallicity of hot gas.

2.5 Star Formation History

Fig. 4 summarizes the direct observational estimates of the star formation rate density of the Universe as a function of redshift, and shows the model predictions for the quiescent and starburst models. The models including only quiescent star formation peak at $z \sim 1.5$ and fall off fairly steeply at higher redshifts, similar to the models of Ref. [1]. The contribution of starburst galaxies to the global star formation rate density is clearly significant at $z \gtrsim 2$. The starburst models exhibit a peak at higher redshift ($z \sim 3$) and are almost flat out to $z \sim 5$. This would appear to be in better agreement with the UV observations derived from Lyman-break galaxies after correction for dust extinction, and with the SCUBA results. The poor behaviour of the models at $z < 1$ is partially due to inaccuracies in the Press-Schechter approximation, and partially a result of our simple assumption of constant quiescent star formation efficiency.

The stars created at high redshift form the population of old stars in present day galaxies. Fig. 5 shows Ω_* as a function of redshift in the quiescent and burst models. Combining the estimate of the present day stellar mass density from Ref. [47] with Renzini’s claim that one third of these stars should be in place by $z = 3$ leads to the estimate that $h\Omega_*(z = 3) = 8 \times 10^{-4}$. If this estimate is correct, the no-burst models, like the models of Ref. [1] or direct integration of the original Madau diagram [7], do not produce enough old stars. The models including starbursts, which are in better agreement with the “new Madau diagram”, also produce an old stellar population that is in good agreement with the “fossil evidence”.

A complementary quantity is the global mass density in the form of cold gas. This can be estimated observationally from the frequency and column densities of damped Lyman- α

systems (DLAS). Fig. 6 shows the fraction of the critical density in the form of cold gas, as estimated from DLAS [11] and as predicted in the models. Note that although the observations only reflect H_I gas in systems with column density greater than $2 \times 10^{20} \text{ cm}^{-2}$, the model predictions are for all cold gas regardless of its form (atomic, ionized, or molecular) or column density. These observations provide an important constraint on the recipes used to model quiescent star formation: we cannot simply increase the efficiency of star formation without limit and still retain enough cold gas to reproduce these observations. At high redshift, we are already starting to push the observed lower limit on the amount of cold gas needed to explain the DLAS observations.

Yet one more indicator of the star formation history is contained in the metal content of the universe, shown in Fig. 7. The mean metallicity of cold gas in DLAS at $z \sim 1 - 3$ has been estimated by [13], and the metallicity of hot gas in clusters has been estimated from X-ray observations [46]. Our treatment of chemical evolution is rather crude, effectively tracing the products of Type II SN only. The effective yield in the models is adjusted in order to attain an average stellar metallicity of about solar at $z = 0$ in Milky Way sized galaxies, and hot gas with $Z \simeq 0.3Z_\odot$ in large halos. The metallicity of the cold gas in the models is not directly constrained but is determined by the feedback and cooling processes. Once again the burst models show milder evolution with redshift, which is directly connected to the flat shape of the star formation history at $z \gtrsim 3$ seen in Fig. 4. Both the quiescent and burst models are probably consistent with the DLAS observations, given that the metallicity of the DLAS may be underestimated by up to a factor of two due to selection effects (M. Pettini, private communication). Increasing the efficiency of quiescent star formation would increase the metallicity of the cold gas at high redshift and violate this constraint, unless a large fraction of the metals are ejected by supernova winds (unlikely except in very small mass dwarf systems [48]). The burst models also predict very little evolution in the metallicity of hot gas out to $z \sim 0.3$, in good agreement with the X-ray observations.

2.6 The Extra-galactic Background Light

The semi-analytic models provide all the necessary information to compute the integrated extra-galactic background light. For this purpose, we have implemented a simple model for dust extinction in which the mass of dust in each galaxy is assumed to be proportional to the mass of metals in the cold gas. We then require that the energy absorbed by dust must be re-radiated according to an assumed dust emission spectrum. The dust models are summarized in [21] and are effectively very similar to those used by Ref. [49], except that we have not attempted to include the heavily extinguished ultra-luminous starburst galaxies which probably contribute significantly to the far IR background [49]. This will require more detailed modelling of dust absorption and re-radiation in starburst galaxies, which we will pursue in future studies. Fig. 8 shows the resulting integrated extra-galactic background light (EBL) for the fiducial SCDM models of Ref. [18]. The contribution to the present day EBL from galaxies at various redshifts is also shown. Apparently, most of the observed EBL is produced by relatively nearby galaxies. This is mainly due to the usual decrease of energy density with the expansion of the universe. The EBL from 0.1 to 2 microns is mainly starlight. At $\lambda \lesssim 1\mu$, a significant portion of the light is absorbed by dust and reradiated in the far-IR. The EBL at $\gtrsim 10\mu$ is almost completely due to re-radiation by dust, and is therefore quite sensitive to our assumed dust absorption and emission models. The characteristic shape of the EBL is also sensitive to the assumed cosmology, star formation history, and IMF [50]. With the wealth of multi-band observations that are now becoming available, the EBL will be an important probe of galaxy formation and cosmology.

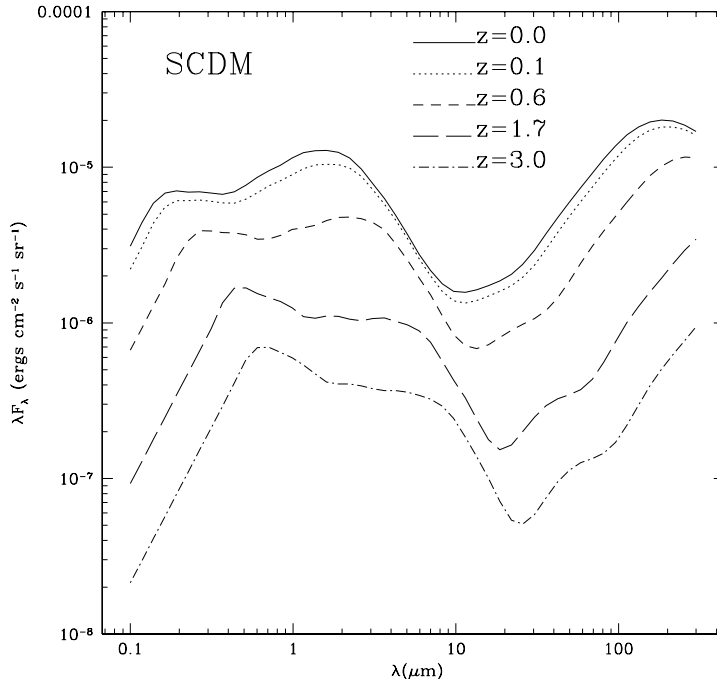


Figure 8: The extra-galactic background light from the far UV to the far IR, for the SCDM model. The dotted and dashed lines show the contribution to the $z = 0$ EBL from galaxies at $z \geq 0.1, 0.6, 1.7,$ and 3.0 as indicated. Most of the observed EBL at the wavelengths shown is produced by relatively nearby galaxies.

2.7 Summary

We have shown that our CDM-based hierarchical models are in good agreement with direct observational estimates of the global star formation history, and are compatible with the fossil evidence which indicates that a significant fraction of the stars in galaxies today formed at high redshift. An important new ingredient in our models is the inclusion of starbursts triggered by galaxy-galaxy interactions. It follows naturally in the CDM picture of structure formation that such starburst events are more common at high redshift, and are also brighter because the gas supply has not yet been depleted. The starburst picture accounts naturally for many of the observed features of the high redshift Lyman-break galaxies, including their number density and luminosity distribution, and also their sizes, star formation rates, colors, ages, and line-widths. In addition, the starburst mode results in a significant modification of the star formation history of the universe, moving the peak in the Madau diagram to higher redshift and leading to a much more gradual decline in the star formation rate out to $z \sim 6$. This is in better agreement with the “new Madau diagram” that results when the considerable dust extinction at $z \gtrsim 3$ now favored by observers is taken into account, and with the SCUBA observations.

Many of the galaxy mergers that trigger starbursts will result in the formation of an early-type galaxy or bulge. Small mass starburst remnants may be accreted by larger galaxies, forming a Pop II halo [51] like that of our own Galaxy [52]. At high redshift ($z \gtrsim 2$), merger events occur mainly in and around massive, strongly clustered dark matter halos. The merger-starburst picture therefore predicts simultaneously the strong observed clustering of the Lyman-break galaxies [33], and that the oldest stars in the universe should be found preferentially in

dense environments today. The mass of old stars ($z_{\text{form}} > 3$) predicted by the starburst models is in good agreement with observational estimates, unlike some previous CDM-based models, which did not produce enough old stars. The gas density and metal content of the universe as a function of redshift, indicated by observations of damped Lyman- α systems, are important complementary constraints on the star formation history and on recipes used to model star formation and supernovae feedback. We present a calculation of the integrated extra-galactic background light, which will be an increasingly important constraint on galaxy formation and the associated processes of dust absorption and re-radiation.

In recent years, our knowledge of the Universe has been considerably extended both in redshift and in wavelength, and no doubt this trend will continue. The interpretation of these exciting observations is subject to many uncertainties due to poorly understood astrophysical processes, notably star formation, dust extinction, and the stellar initial mass function. We argue that the best approach to overcoming these problems is to investigate many different kinds of constraints. We conclude that the CDM framework, as realized by the complementary techniques of simulations and semi-analytic models of galaxy formation, can account for the current observations and provides an excellent basis for continuing study of these issues.

Acknowledgments

We thank our collaborators George Blumenthal, James Bullock, Avishai Dekel, S.M. Faber, Michael Gross, Patrik Jonsson, Anatoly Klypin, Tsafir Kolatt, Andrey Kravtsov, Yair Sigad, Ian Walker, and Risa Wechsler for allowing us to report on our new work here. JRP acknowledges support from NASA and NSF grants at UCSC, and a Forchheimer Visiting Professorship at Hebrew University. RSS acknowledges support from a NASA grant and a GAANN Fellowship at UCSC and a University Fellowship from the Hebrew University, Jerusalem.

References

- [1] C.M. Baugh et al. 1998, ApJ, 498, 504
- [2] J. Gallego et al. 1995, ApJ, 455, L1
- [3] L. Tresse, S.J. Maddox 1997, *The Young Universe*, ed. S. D’Odorico, A. Fontana, E. Giallongo, ASP Conf. Series (astro-ph/9712130)
- [4] C. Gronwall 1998, *Dwarf Galaxies and Cosmology*, eds. Thuan et al., Editions Frontieres, in press (astro-ph/9806240)
- [5] D. Hogg et al. 1998, ApJ in press, (astro-ph/9804129)
- [6] S.J. Lilly et al. 1996, ApJ, 460, L1
- [7] P. Madau et al. 1996, 283, 1388; P. Madau 1996, 7th Annual October Astrophysics Conference in Maryland, “Star Formation Near and Far” (astro-ph/9612157)
- [8] M.A. Treyer et al. 1997, *The Ultraviolet Universe at Low and High Redshift*, ed. W. Waller, Woodbury: AIP Press (astro-ph/9706223)
- [9] D. Hughes et al. 1998, Nature, 394, 241
- [10] K.M. Lanzetta, A.M. Wolfe and D.A. Turnshek 1995, ApJ, 440, 435
- [11] L.J. Storrie-Lombardi, R.G. McMahon, M.J. Irwin 1996, MNRAS, 283, 79L
- [12] S.M. Fall, Y.C. Pei, S. Charlot 1996, 464, 43L
- [13] M. Pettini et al. 1997, ApJ, 486, 665
- [14] E. Dwek et al. 1998, ApJ, in press (astro-ph/9806129)

- [15] A. Renzini 1997, ApJ, 488, 35; A. Renzini 1998, in *The Young Universe*, ed. S. D'Odorico, A. Fontana, E. Giallongo, ASP Conf. Series (astro-ph/9801209)
- [16] G. Kauffmann, S.D.M. White, B. Guiderdoni 1993, MNRAS, 264, 201
- [17] S. Cole et al. 1994, MNRAS, 271, 781
- [18] R.S. Somerville, J.R. Primack 1998, MNRAS in press (astro-ph/9802268)
- [19] M.J. Sawicki, H. Lin, H.K.C. Yee 1997, AJ, 113, 1
- [20] R.S. Somerville, J.R. Primack, S.M. Faber 1998, MNRAS, in press (astro-ph/9806228)
- [21] R.S. Somerville 1997, Ph.D. thesis, UCSC (www.fiz.huji.ac.il/~rachels/thesis.html)
- [22] R.S. Somerville, T.S. Kolatt 1998, MNRAS, in press (astro-ph/9711080)
- [23] S. Charlot, A. G. Bruzual 1993, ApJ, 405, 538
- [24] J.C. Mihos, L. Hernquist 1994, ApJ, 425, L13; *ibid* 1996, ApJ, 464, 641
- [25] J. Makino, P. Hut 1997, ApJ, 481, 83
- [26] M. Pettini et al. 1997, ApJ, 478, 536
- [27] M. Dickinson, in *The Hubble Deep Field*, ed. M. Livio et al. (astro-ph/9802064)
- [28] D. Calzetti, in *The Ultraviolet Universe at Low and High Redshift*, ed. W. Waller
- [29] K.L. Adelberger et al. 1998, ApJ, 505, 18
- [30] L. Pozzetti et al. 1998, MNRAS, in press (astro-ph/9803144)
- [31] G. Meurer et al. 1997, AJ, 114, 54
- [32] M. Sawicki, H.K.C. Yee 1998, AJ, 115, 1329
- [33] T. Kolatt et al. 1998, in prep.
- [34] A.V. Kravtsov, A.A. Klypin, A.M. Khokhlov 1997, ApJS 111, 73
- [35] I. Walker et al. 1998, in prep.
- [36] M. Pettini et al. 1998, ApJ, in press (astro-ph/9806219)
- [37] C.C. Steidel et al. 1998, ApJ, 492, 428
- [38] M. Giavalisco et al. 1998, ApJ, in press (astro-ph/9802318)
- [39] R.H. Wechsler et al. 1998, ApJ, in press (astro-ph/9712141)
- [40] Y.P. Jing, Y. Suto 1998, ApJ, 494, L5
- [41] P. Madau, L. Pozzetti, M. Dickinson 1998, ApJ, 498, 106
- [42] A.J. Connolly et al. 1997, ApJ, 486, 11L
- [43] M.A.K. Gross et al. 1998, MNRAS in press (astro-ph/9712142)
- [44] R.S. Somerville et al. 1998, astro-ph/9807277
- [45] M.A. Zwaan et al. 1997, ApJ, 490, 173
- [46] R.F. Mushotszky, M. Loewenstein 1997, ApJ, 481, 63L
- [47] M. Fukugita et al. 1998, ApJ, 503, 518
- [48] M.-M. Mac Low, A. Ferrera 1998, ApJ, in press (astro-ph/9801237)
- [49] B. Guiderdoni et al. 1998, MNRAS, 295, 877
- [50] J. Bullock et al. 1998, in prep.
- [51] S.C. Trager et al. 1998, ApJ, 485, 92
- [52] K.V. Johnston et al. 1996, ApJ, 465, 278